JVI Journals.ASM.org

Hepatitis A Virus Adaptation to Cellular Shutoff Is Driven by Dynamic Adjustments of Codon Usage and Results in the Selection of Populations with Altered Capsids

M. Isabel Costafreda,[a,c] Francisco J. Pérez-Rodriguez,[a,c] Lucía D'Andrea,[a,c] Susana Guix,[a,c] Enric Ribes,[b] Albert Bosch,[a,c] Rosa M. Pintó[a,c]

Enteric Virus Laboratory, Department of Microbiology, School of Biology,[a] Enteric Virus Laboratory, Department of Cell Biology, School of Biology,[b] and Institute of Nutrition and Food Safety,[c] University of Barcelona, Barcelona, Spain

ABSTRACT

Hepatitis A virus (HAV) has a highly biased and deoptimized codon usage compared to the host cell and fails to inhibit host protein synthesis. It has been proposed that an optimal combination of abundant and rare codons controls the translation speed required for the correct capsid folding. The artificial shutoff host protein synthesis results in the selection of variants containing mutations in the HAV capsid coding region critical for folding, stability, and function. Here, we show that these capsid mutations resulted in changes in their antigenicity; in a reduced stability to high temperature, low pH, and biliary salts; and in an increased efficacy of cell entry. In conclusion, the adaptation to cellular shutoff resulted in the selection of large-plaque-producing virus populations.

IMPORTANCE

HAV has a naturally deoptimized codon usage with respect to that of its cell host and is unable to shut down the cellular translation. This fact contributes to the low replication rate of the virus, in addition to other factors such as the highly inefficient internal ribosome entry site (IRES), and explains the outstanding physical stability of this pathogen in the environment mediated by a folding-dependent highly cohesive capsid. Adaptation to artificially induced cellular transcription shutoff resulted in a redeoptimization of its capsid codon usage, instead of an optimization. These genomic changes are related to an overall change of capsid folding, which in turn induces changes in the cell entry process. Remarkably, the adaptation to cellular shutoff allowed the virus to significantly increase its RNA uncoating efficiency, resulting in the selection of large-plaque-producing populations. However, these populations produced much-debilitated virions.

Translation accuracy has been defined as the probability that the translated protein will match the sequence prescribed in the encoding gene combined with the likelihood that it will fold properly (1). Translation and folding of newly synthesized proteins are coupled events, and precise mechanisms of adjustment between the two processes exist. Translation speed has been proposed as one such mechanism (2) and may be regulated through the mRNA structure and the combination of abundant and rare codons (3). Abundant codons usually match with highly concentrated tRNAs, contributing to both efficiency of translation (they are rapidly translated) and accuracy of translation (they are high-fidelity codons) (1). In contrast, rare codons are slowly translated and are of low fidelity due to erroneous incorporations of near-cognate tRNAs during the long search for the scarce cognate tRNAs (1, 4, 5). Selection should prefer high-fidelity abundant codons at sites at which translation errors are structurally disruptive, such as buried residues and/or residues at sites where mutations lead to large changes in free energy (6). At the same time, clusters of low-fidelity rare codons, which act as translation attenuation patterns, caused by ribosome pauses, are preserved across species, suggesting a concerted selective pressure on codon matching and species-specific tRNA abundance in these regions (7, 8). In other words, to maintain protein function, from an evolutionary perspective it may be more critical to preserve translation attenuation patterns than to preserve amino acid sequences, a clear illustration of a noncoding functional sequence conservation (9). Several examples in prokaryotic and eukaryotic genomes suggest a critical role of rare codons in protein folding and function (2, 7). In *Escherichia coli*, the folding efficiency of the multidomain protein SufI can be severely perturbed by alterations in ribosome-mediated translational attenuation at rare codons (10, 11). In humans, the P-glycoprotein encoded in the MDR1 (or ABCB1) gene shows an altered conformation when a silent mutation is present which affects the timing of cotranslational folding and insertion of the protein into the membrane (12).

Hepatitis A virus (HAV) does not inhibit the cellular protein synthesis and competes poorly with cellular mRNAs for the translational machinery (13). The initiation of translation in HAV is inefficient, and the virus uses a highly deoptimized codon repertoire (14–16). HAV uses as rare codons those that are rare in the cell codon usage but also those that are highly abundant and whose cognate tRNAs may be unavailable for the virus due to its incapacity to shut down the cellular protein synthesis. Recently, we have described how HAV adapts to grow under conditions of artificially induced cellular protein shutoff, adjusting its codon

Received 10 January 2014 **Accepted** 13 February 2014
Published ahead of print 19 February 2014
Editor: K. Kirkegaard
Address correspondence to Rosa M. Pintó, rpinto@ub.edu.

doi:10.1128/JVI.00087-14

usage (17). Overall, adaptation to conditions of cellular shutoff correlated with a redeoptimization of the codon usage in the capsid coding region, suggesting a critical need for a slow translation pace in this specific genomic region (17). Our data suggest that proper folding of HAV capsid relies on the kinetics of translation controlled by pauses at clusters of rare codons rather than the chaperons used by other picornaviruses (17–19). However, the direct influence of codon frequency class usage adjustments on capsid folding (here referred to as codon usage changes) was not directly revealed.

In the present work, we studied mutations that affected HAV capsid folding selected under different degrees of cellular translation shutoff and analyzed the implications of the capsid folding changes for antigenic structure, stability under extreme conditions, and initiation of the replicative cycle. Cellular shutoff was based on transcription shutoff and was achieved by using actinomycin D (AMD), which specifically inhibits the DNA-dependent RNA polymerases with no effect on the RNA-dependent RNA polymerases (20). This cellular transcription shutoff might be associated with a low cellular protein synthesis, and hence, an increase of the tRNA pool available for the virus would be expected. Direct evidence of the critical role of codon usage in both folding and biological properties of HAV capsid and, in turn, in the selection of large-plaque-producing populations is provided.

MATERIALS AND METHODS

Cells and viruses. The cytopathogenic pHM175 43c strain of HAV was used for the study of HAV replication and evolution in the presence of actinomycin D (AMD; Sigma). AMD, at concentrations of 0.05 μg/ml and 0.2 μg/ml, was added in the postinfection medium to inhibit DNA transcription of the infected FRhK-4 cells at levels of around 60 to 70% and over 90%, respectively (17). A total of 12 populations were used throughout this study. The following nomenclature is used: F, forward adaptation; R, reverse adaptation; NA, nonadapted; A, adapted; and LA, long adapted. The included populations were the parental population growing in 0.0 μg/ml (L0; P5-AMD), the population growing in the presence of 0.05 μg/ml of AMD but still nonadapted to the drug (F0.05NA; P5 + 0.05AMD), the same population after adaptation (F0.05A; P60 + 0.05AMD) to this AMD concentration, the same population after a long period of adaptation (F0.05LA; P120 + 0.05AMD), the population F0.05A in its reversion to the absence of the drug before (R0NA; P85 + 0.05AMD/P5-AMD) and after (R0A; P85 + 0.05AMD/P20-AMD) adaptation to this new condition, the population growing in the presence of 0.2 μg/ml of AMD but still nonadapted to the drug (F0.2NA; P85 + 0.05AMD/P5 + 0.2AMD), the same population after adaptation (F0.2A; P65 + 0.05AMD/P40 + 0.2AMD) to this AMD concentration, the same population after a long period of adaptation (F0.2LA; P65 + 0.05AMD/P70 + 0.2AMD), and the population F0.2LA in its reversion to the 0.05 μg/ml of AMD before (R0.05NA; P65 + 0.05AMD/P70 + 0.2AMD/P5 + 0.05A) and after (R0.05A; P65 + 0.05AMD/P70 + 0.2AMD/P20 + 0.05A) adaptation to this new condition. Most of these populations, with the exception of the long-adapted populations and those reverting to 0.05 μg/ml of AMD, had been previously described (17). A workflow diagram of the history and relationship between these populations is shown in Fig. 1.

Infections were carried out in the FRhK-4 cell line under each specific AMD condition, and progenies were recovered between 5 and 7 days after infection as previously described (17). The infectious virus titers (50% tissue culture infective doses [$TCID_{50}$]) were also obtained in FRhK-4 cell monolayers in the absence of AMD. Genome copy numbers were determined using a previously described standardized quantitative PCR (qPCR) method which includes both RNA extraction and reverse transcription-PCR (RT-PCR) inhibition controls (21–23). Five microliters of samples was boiled and used in a one-step real-time RT-PCR based on the amplification of a fragment from the 5′ noncoding region (NCR) (21). Virus and genome copy yields per cell were calculated taking into consideration the average cell viabilities at days 4, 5, 6, and 7, which were 78% and 9% for 0.05 μg/ml and 0.2 μg/ml of AMD, respectively.

Plaque assays were also performed in FRhK-4 cells as previously described (24), in the absence or in the presence of 0.05 μg/ml of AMD, which was added to the agarose overlay medium. The highest concentration, 0.2 μg/ml, of AMD was not tested due to its high toxicity at 10 days postinfection when monolayers were fixed with 4% formaldehyde and stained with crystal violet.

Production of concentrated viral stocks. Suspensions with high virus concentration were used for the analysis of recognition by different monoclonal antibodies (MAbs).

For each population, concentrated viral stocks were obtained as previously described (25). Briefly, at 5 to 6 days postinfection under each specific condition of AMD, infected cells (multiplicity of infection [MOI] of 1) from a T-175 flask were harvested by trypsin treatment, collected by centrifugation, resuspended in 500 μl of NT buffer (0.1 M NaCl, 10 mM Tris-HCl, 1% NP-40, pH 7.4), and incubated for 30 min at room temperature. These lysed cell suspensions were centrifuged at 1,700 × *g* for 5 min, and the supernatants were again centrifuged at 13,000 × *g* for 5 min. Viruses recovered in the supernatants were subjected to three sonication cycles of 30 s at 60 W in the presence of 0.4% SDS.

Recognition by H7C27, K34C8, and K24F2 monoclonal antibodies. Recognition of HAV particles from the different populations with MAbs H7C27, K34C8, and K24F2 was tested. H7C27 MAb recognizes the glycophorin A binding site (26, 27), while K34C8 and K24F2 MAbs are directed against the immunodominant site (26). While K24F2 and H7C27 epitopes are present in the protomers, procapsids, and capsids, the epitope recognized by the K34C8 MAb is present only in procapsids and capsids (28). For the recognition with each individual MAb, a sandwich enzyme-linked immunosorbent assay (ELISA) was performed (29), in which particles were captured by a convalescent-phase serum and detected with H7C27, K34C8, or K24F2 MAb. All MAbs were used at the highest dilution yielding recognition of the pHM175 43c strain of HAV. This strain, although resistant to neutralization by MAb K24F2 (26), still shows antibody binding (30) and is well recognized by ELISA at a high concentration of the antibody (31). Thus, the dilutions used were 1/10,000 for H7C27 and K34C8 MAbs and 1/250 for K24F2 MAb. An average of 1.5×10^6 $TCID_{50}$ per well was used. Mock-infected FRhK-4 cell extracts were used as negative controls. Three different stocks for each population were tested.

Resistance to high temperature, acid pH, and biliary salts. Treatments at 61°C for 5 min, pH 2 for 1 h at 37°C, and 1% biliary salts for 4 h at 37°C were performed, and the resistance of each population was evaluated. To quantify virus decay, a control test of nontreated viruses kept for the same length of time at 37°C was run in parallel. The $\log_{10}$ reduction of the virus titer after each treatment compared with the infectious titer of the parallel nontreated virus control was determined. Three different stocks for each population were tested.

Determination of cell binding capacity. Cell binding capacity was estimated by figuring the difference in infectious virus titer of added inocula on monolayers of FRhK-4 cells (MOI of 1) between 0 and 120 min of adsorption. This difference, expressed as percentage of the initial titer, was used as an estimation of the cell binding capacity. Three different stocks for each population were tested.

Determination of RNA uncoating time. The classical method of virus replication in the presence of neutral red was used to determine the RNA uncoating time of the different populations (32). Briefly, neutral red is incorporated into capsids of viruses grown in its presence, which become photosensitive. Intact viruses remain viable while kept in the dark; however, in the presence of light their RNA is inactivated. When RNA is already uncoated, viruses are no longer photosensitive. Thus, light treatments of viruses at different times after adsorption may be used as a measure of the uncoating process. Virus stocks in the presence of 0.001%

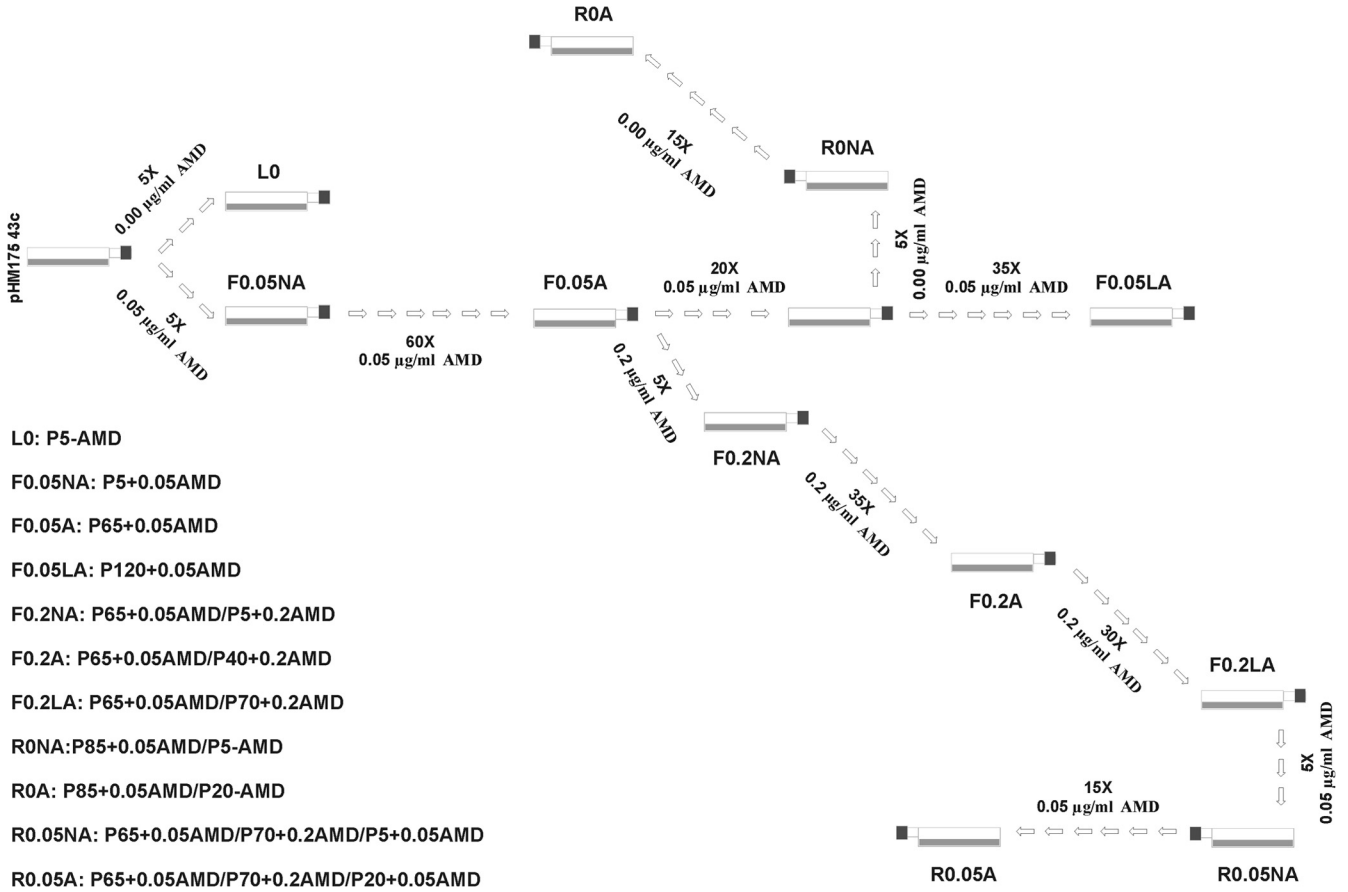

FIG 1 Workflow of the processes of adaptation to changing cellular shutoff conditions, including forward adaptation to 0.05 μg/ml of AMD (F0.05NA still-nonadapted, F0.05A adapted, and F0.05LA long-adapted populations) and to 0.2 μg/ml of AMD (F0.2NA still-nonadapted, F0.2A adapted, and F0.2LA long-adapted populations), as well as the reversion to absence (R0NA still-nonadapted and R0A adapted populations) and 0.05 μg/ml (R0.05NA still-nonadapted and R0.05A adapted populations) of AMD, respectively.

neutral red and the corresponding AMD concentration were produced for each population in absolute darkness by infecting FRhK-4 cell monolayers at an MOI of 1. At 5 days postinfection, cells were lysed by three cycles of freeze-thawing at −80°C and cell debris was removed by low-speed centrifugation. Viruses present in the supernatant were titrated by the $TCID_{50}$ as described above, and seven replicas were made, each corresponding to time zero and 1, 3, 6, 9, 12, and 24 h after adsorption when microtiter plates were lit up. All manipulations were done under red light. The time when RNA was uncoated in 50% of the virus population (UT_{50}) was estimated from the time kinetics. Three different stocks for each population were tested.

Determination of specific infectivity. Specific infectivity was determined in supernatants of infected cells as an indication of the number of viruses required to achieve an infectious cycle. FRhK-4 cell monolayers were infected with the different populations at an MOI of 0.1, and culture medium supernatants were collected at 5 days postinfection. Cell debris was removed through a two-step centrifugation (1,700 × *g* for 5 min followed by 13,000 × *g* for 5 min), and the resulting supernatants were analyzed. Specific infectivity in these culture medium supernatants was figured by dividing the number of infectious units by the number of genome copies per ml. Infectious units and genome copies were determined as described above. Three different stocks for each population were tested.

Genomic analysis. Codon and anticodon usages of each viral population were inferred through the analysis of the sequences of 50 molecular clones of two capsid genomic regions (comprising codons 1 to 123 of VP3 and 85 to 245 of VP1) and compared with codon and anticodon usage of the host cell as previously described (17, 33). Anticodon usage variation was estimated through codon usage variation assuming a model based on the frequency of the codons, the anticodon degeneracy, and the codon-anticodon match pairing preferences (17, 33). Anticodons were sorted into two groups: those used by the cell at a frequency between 0 and 60% and those used at a frequency between 60 and 100%. The relative usage variation of each anticodon compared with the initial L0 population for each population was figured. The dinucleotide content, particularly CpG and UpA, was also analyzed to look for variations in their number during the process of adaptation to cellular shutoff.

Additionally, a bioinformatic analysis to screen for all potential mutations in the complete capsid coding region of the pHM175 43c strain was undertaken. Mutations were first classified as synonymous (Syn) or nonsynonymous (NSyn) and as transitions (T_s) or transversions (T_v). Any mutation induces a codon change, and the newly generated codons were further sorted as being similarly frequent (within a 10% range), less frequent (below 10%), or more frequent (above 10%) than the original ones with respect to the cell host codon usage, as an indication of the adaptation to the cellular tRNA pool. The relationship between mutation type and the change to a new codon used at a different frequency by the host cell was figured.

Statistical analysis. Global statistical differences between the different virus populations regarding ratios of MAb recognition, physical stability, cell binding capacity, uncoating times, fitness, ratios between different virus particles, specific infectivity, and plaque size were assessed by using the analysis of variance (ANOVA). Particular differences between pairs of

TABLE 1 Recognition of the different HAV populations by monoclonal antibodies H7C27, K34C8, and K24F2

Population[a]	Absorbance (mean ± SE) for MAb[b]:		
	H7C27	K34C8	K24F2
L0	0.20 ± 0.001 A	0.22 ± 0.001 A	0.28 ± 0.002 A
F0.05NA	0.17 ± 0.001 A	0.20 ± 0.0002 A	0.22 ± 0.004 B
F0.05A	0.19 ± 0.001 A	0.20 ± 0.002 A	0.22 ± 0.004 B
F0.05LA	0.37 ± 0.005 B	0.89 ± 0.03 B	0.12 ± 0.005 C
F0.2NA	0.19 ± 0.001 A	0.20 ± 0.002 A	0.19 ± 0.003 B
F0.2A	0.46 ± 0.005 C	0.28 ± 0.002 C	0.27 ± 0.002 A
F0.2LA	0.25 ± 0.004 A	0.25 ± 0.002 A, C	0.18 ± 0.006 B
R0NA	0.37 ± 0.007 B	0.95 ± 0.005 B	0.12 ± 0.003 C
R0A	0.33 ± 0.009 B	0.90 ± 0.005 B	0.10 ± 0.030 C
R0.05NA	0.37 ± 0.010 B	0.99 ± 0.006 B	0.12 ± 0.002 C
R0.05A	0.36 ± 0.009 B	1.02 ± 0.004 B	0.11 ± 0.003 C

[a] Populations included are described in Fig. 1.
[b] Values represent the mean ± standard error of ELISA absorbance values of three different virus stocks. Statistically significant differences ($P < 0.001$) between pairs of populations are indicated by different letters; populations with the same letter are not significantly different.

populations were assessed using the Student *t* test (unpaired). Results are expressed as the mean ± standard error of at least three independent experiments.

Nucleotide sequence accession numbers. Consensus sequences of the different selected populations have been deposited in GenBank with accession numbers KF724017 to KF724023.

RESULTS

Capsid folding is dependent on cellular shutoff conditions. We analyzed whether changes in codon usage during selection under cellular translation shutoff induced folding changes in the HAV capsid. To do so, we studied the antigenicity and stability of the capsid in HAV populations adapted or not to different shutoff conditions. L0 and F0.05A populations were used as baseline controls for the process of adaptation to 0.05 and 0.2 μg/ml of AMD, respectively (Fig. 1). Similarly, F0.05A and F0.2LA populations were the controls for the reversion processes to absence and 0.05 μg/ml of AMD, respectively (Fig. 1).

The antigenic structure was analyzed through the recognition by H7C27, K34C8, and K24F2 MAbs (Table 1). The ratio between the recognition with H7C27 and K24F2 MAbs and K34C8 and K24F2 MAbs was also calculated to normalize differences in antigen yields among the populations as well as interassay variations (Fig. 2). The adaptation to grow in 0.05 μg/ml (Fig. 2A and E) and 0.2 μg/ml (Fig. 2C and G) of AMD resulted in the selection of viral populations with significantly different antigenicities ($P < 0.001$) as assessed by the increase in the H7C27/K24F2 (Fig. 2A and C) and K34C8/K24F2 (Fig. 2E and G) MAb reaction ratios. The same pattern of significant ($P < 0.001$) increases of these ratios was also observed during the reverse processes from 0.05 μg/ml of AMD to absence (Fig. 2B and F) and from 0.2 μg/ml to 0.05 μg/ml of AMD (Fig. 2D and H). As a general rule, increases in the H7C27/K24F2 ratio were mainly due to both a significant increase ($P < 0.001$) of recognition by MAb H7C27 and a significant decrease ($P < 0.001$) of recognition by MAb K24F2, with the exceptions of population F0.2A, which showed only a significant increase ($P < 0.001$) of recognition by MAb H7C27, and populations F0.05A and F0.2LA, which showed only a significant decrease ($P < 0.001$) of recognition by MAb K24F2 (Table 1). Similarly, in the case of the K34C8/

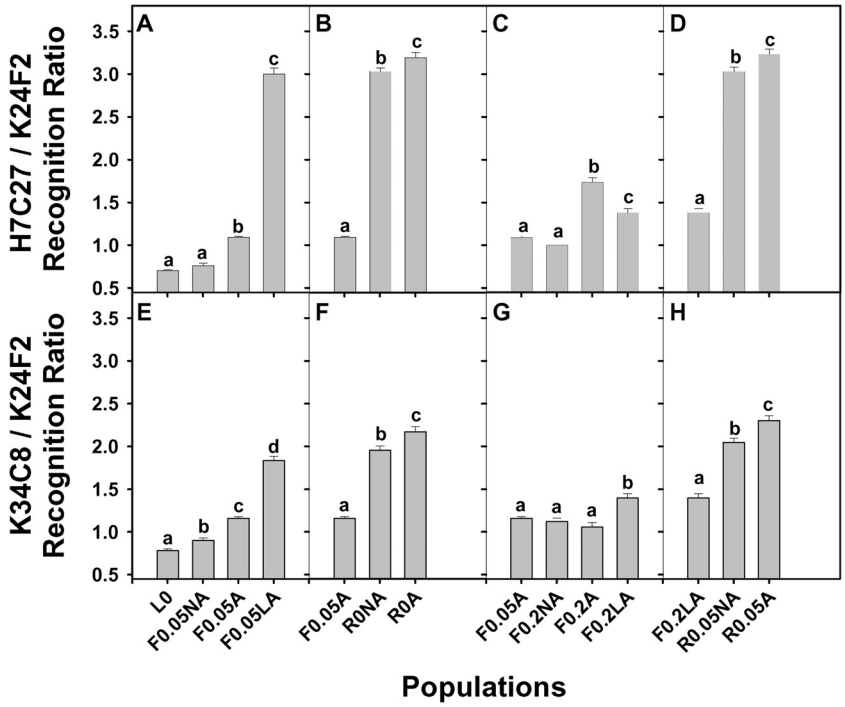

FIG 2 Changes in capsid folding measured through the analysis of the antigenic structure of the different populations selected during the processes of adaptation to changing AMD concentrations. (A through D) Ratio between virus recognition by MAb H7C27 and that by MAb K24F2. (E through H) Ratio between virus recognition by MAb K34C8 and thab by MAb K24F2. Populations tested are described in Fig. 1. Values represent the mean ± standard error of three different virus stocks. Statistically significant differences ($P < 0.001$) between pairs of populations within each panel are indicated by different letters; populations with the same letter are not significantly different.

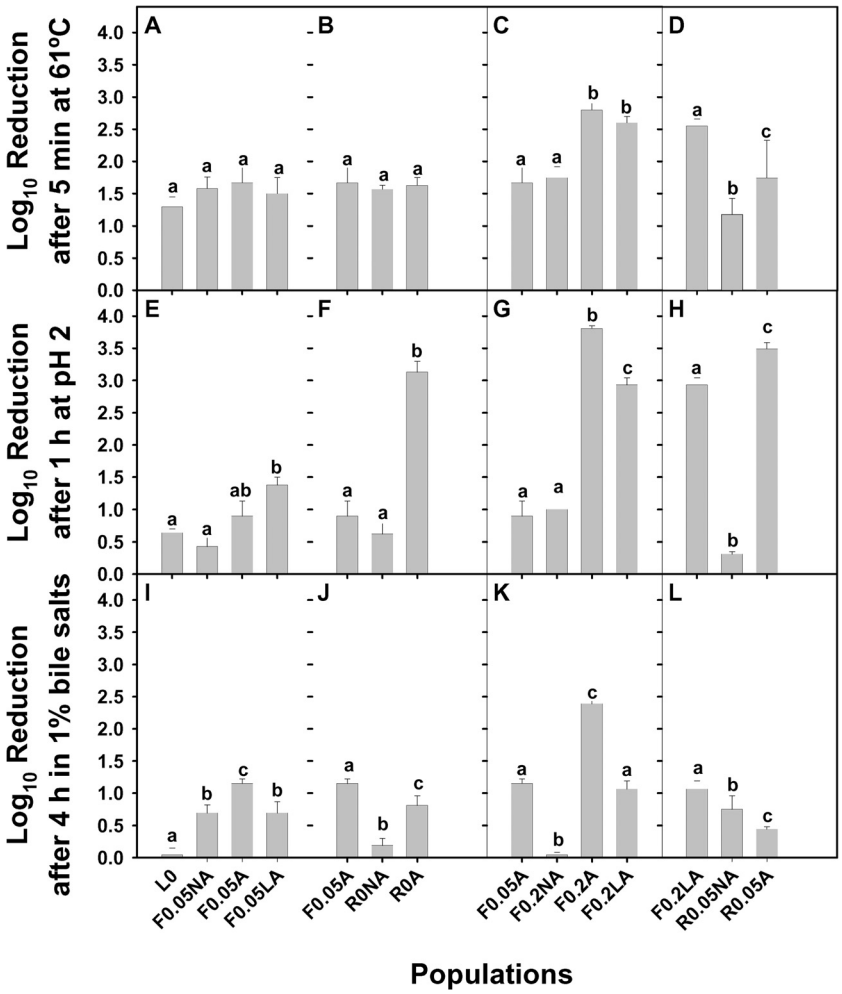

FIG 3 Changes in capsid folding measured through the analysis of the stability under extreme conditions of the different populations selected during the processes of adaptation to changing AMD concentrations. (A through D) Virus stability after 5 min at 61°C. (E through H) Virus stability after 1 h at pH 2. (I through L) Virus stability after 4 h in the presence of 1% bile salts. Stability under a particular treatment was measured as the loss of virus infectivity due to this treatment, and it is expressed as the $\log_{10}$ reduction. Populations tested are described in Fig. 1. Values represent the mean ± standard error of three different virus stocks. Statistically significant differences (particular *P* levels are described in the text) between pairs of populations within each panel are indicated by different letters; populations with the same letter are not significantly different.

K24F2 ratio, increases were mainly due to a concomitant increase of the recognition by MAb K34C8 and a decrease of recognition by MAb K24F2 (Table 1) with the exceptions of populations F0.05NA, F0.05A, and F0.2LA, which showed only a significant decrease ($P < 0.001$) of recognition by MAb K24F2 (Table 1).

Many of the mutations inducing codon usage changes during the process of adaptation also induced amino acid replacements (F0.05A, S134G and I85V in VP2 and VP1, respectively; F0.05LA, A12E in VP3; F0.2A, I142M in VP3; F0.2LA, S43P in VP1; sequences available at GenBank), which in turn may be the reason for the changes in antibody recognition. However, none of the detected amino acid replacements were located at the described epitopes. On the other hand, several observations indicate that codon-usage-driven capsid folding changes could, at least in part, contribute to alterations in the immunological recognition. Non-adapted populations showed no "fixed" mutations of any kind, and in the quasispecies, only a few mutations were detected, which did not produce significant changes in codon usage. However, these populations showed altered recognition patterns anyway. Highly evident examples are F0.05A/R0NA and F0.2LA/R0.05NA pairs of populations, which in spite of being practically identical at the genomic level showed very important and significantly ($P < 0.001$) different recognition patterns (Table 1 and Fig. 2B, D, F, and H). In both cases, changes in the growing conditions (from 0.05 μg/ml of AMD to absence of the drug and from 0.2 μg/ml to 0.05 μg/ml of AMD) strongly influenced capsid folding.

The physical stability of the different populations under extreme conditions was also tested, including stability at 61°C for 5 min, at pH 2 for 1 h at 37°C, and in the presence of 1% biliary salts for 4 h at 37°C. The adaptation process to 0.05 μg/ml of AMD induced a significant titer reduction in the presence of bile salts (Fig. 3I; $P < 0.001$) and acid pH (Fig. 3E; $P < 0.05$). During the process of return from 0.05 μg/ml of AMD to absence of the drug, a population with a very low stability to acid pH (Fig. 3F; $P < 0.001$) was selected. In contrast, during this return process, the stability of populations to bile salts significantly ($P < 0.05$) increased (Fig. 3J). Stability to high temperature remained stable during these two processes. Adaptation to 0.2 μg/ml of AMD in-

TABLE 2 Fitness, specific infectivities, and plaque diameters of the different HAV populations[e]

Population[a]	$Log_{10}(TCID_{50}/cell)$[b]	Specific infectivity[c]	Diam (cm)[d]
L0	1.43 ± 0.04 A	0.04 ± 0.01 A (1/25)	0.20 ± 0.02 A
F0.05NA	0.73 ± 0.12 B	0.08 ± 0.02 A (1/12)	0.33 ± 0.04 B
F0.05A	1.54 ± 0.08 A	0.12 ± 0.03 B (1/8)	0.61 ± 0.03 C
F0.05LA	1.64 ± 0.05 A	0.07 ± 0.03 A, B (1/14)	0.61 ± 0.04 C
F0.2NA	1.07 ± 0.13 B, C	0.05 ± 0.02 A (1/20)	0.44 ± 0.05 D
F0.2A	1.70 ± 0.12 A	0.44 ± 0.12 C (1/2)	0.73 ± 0.03 E
F0.2LA	1.39 ± 0.14 A, B	0.04 ± 0.02 A (1/20)	0.71 ± 0.04 E
R0NA	1.01 ± 0.17 B	0.43 ± 0.14 C (1/2)	0.49 ± 0.03 D
R0A	1.70 ± 0.12 A	0.36 ± 0.12 C (1/3)	0.56 ± 0.03 C, D
R0.05NA	0.85 ± 0.25 C	0.32 ± 0.05 C (1/3)	0.59 ± 0.04 C
R0.05A	1.60 ± 0.18 A	0.26 ± 0.01 C (1/4)	0.55 ± 0.06 C, D

[a] Populations included are described in Fig. 1.
[b] Fitness was measured as infectious virus production per cell, expressed as $\log_{10}$ of $TCID_{50}$. Significance, $P < 0.05$.
[c] Specific infectivity was estimated by dividing the number of infectious particles by the number of genomes in the supernatant of infected cells. Numbers in parentheses are the average number of infectious particles per the number of physical particles. Significance, $P < 0.01$.
[d] Average diameter of 20 plaques. Significance, $P < 0.001$.
[e] Values represent the mean ± standard error of three different virus stocks. Statistically significant differences between pairs of populations are indicated by different letters; populations with the same letter are not significantly different.

duced significant titer reductions at high temperature (Fig. 3C; $P < 0.001$) and acid pH (Fig. 3G; $P < 0.001$) and significant changes of stability to bile salts (Fig. 3K; $P < 0.001$) but with no clear patterns of increase or decrease. During the process of return from 0.2 μg/ml of AMD to 0.05 μg/ml of AMD, stability to high temperature (Fig. 3D) and bile salts (Fig. 3L) significantly increased ($P < 0.05$). Stability under acid pH (Fig. 3H) first significantly increased ($P < 0.001$) and thereafter significantly decreased ($P < 0.05$).

All these results confirmed the occurrence of capsid folding changes associated with changing cellular shutoff conditions.

The dynamics of the cell entry process is dependent on cellular shutoff conditions. The consecutive adaptation of HAV, first to low (0.05-μg/ml AMD) and thereafter to high (0.2-μg/ml AMD) cellular shutoff conditions (Fig. 1), was always associated with important fitness losses, in terms of virus production (F0.05NA versus L0 and F0.2NA versus F0.05A populations; Table 2), which were subsequently recovered (F0.05A versus L0 and F0.2A versus F0.05A populations; Table 2). This dynamics of fitness loss followed by fitness recovery was not exclusive of the process of adaptation to increasing levels of cellular shutoff. In fact, it was also observed in the reverting processes from 0.05 μg/ml AMD to absence of the drug (R0NA versus F0.05A and R0A versus F0.05A; Table 2) and from 0.2 μg/ml AMD to 0.05 μg/ml AMD (R0.05NA versus F0.02LA and R0.05A versus F0.02LA; Table 2).

Since capsid folding may be critical for the initiation of the replicative cycle and this initiation in turn may affect the overall fitness, both receptor interaction and uncoating patterns of the different populations were analyzed as essential steps of the entry process.

During the process of adaptation to 0.05 μg/ml of AMD, there were significant changes in the efficiency of interaction with the receptor that could explain fitness changes (Fig. 4 and Table 2). The nonadapted F0.05NA population showed a statistically signif-

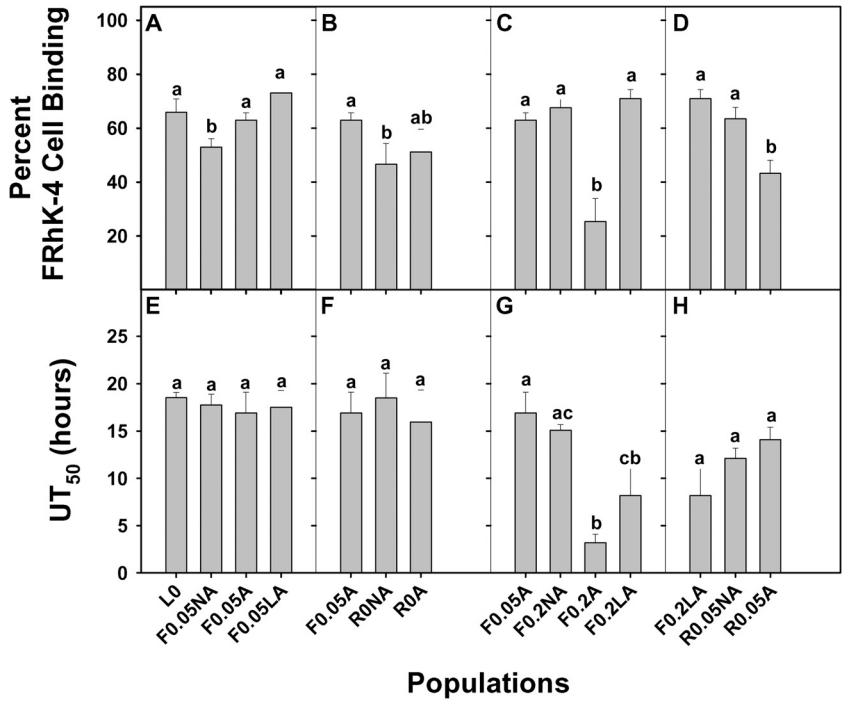

FIG 4 Efficiency of the cell entry process of the different populations selected during the processes of adaptation to changing AMD concentrations. (A through D) Percent binding to FRhK-4 cells. (E through H) Uncoating time 50 (UT_{50}), or the required time for an uncoating of 50% of the virus population, in hours. Populations tested are described in Fig. 1. Values represent the mean ± standard error of three different virus stocks. Statistically significant differences (particular *P* levels are described in the text) between pairs of populations within each panel are indicated by different letters; populations with the same letter are not significantly different.

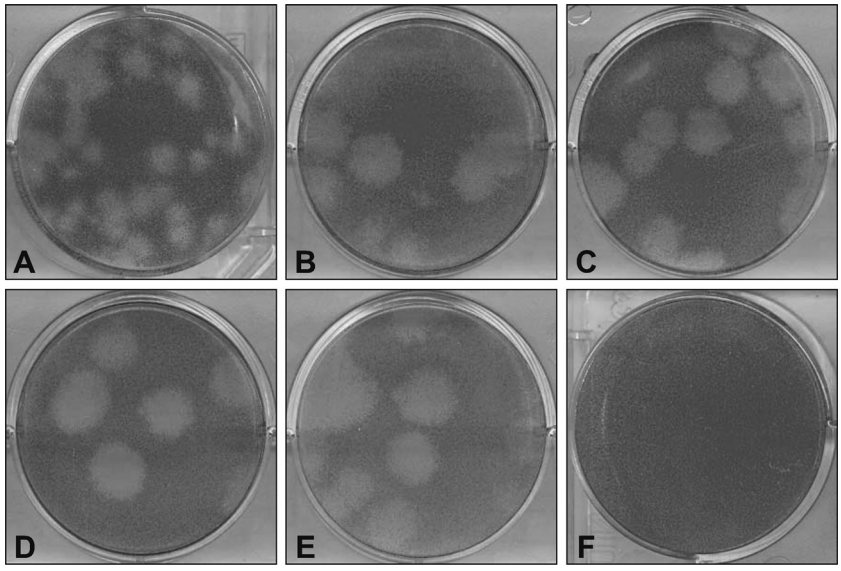

FIG 5 Plaques of the populations adapted to different AMD concentrations. (A) L0; (B) F0.05A; (C) F0.05LA; (D) F0.2A; (E) F0.2LA; (F) mock-infected cells. Populations are described in Fig. 1.

icant ($P < 0.05$) decrease of binding to FRhK-4 cells compared with the parental L0 population (Fig. 4A) as well as a significant decrease ($P < 0.001$) of the virus production per cell (Table 2), while the adapted F0.05A population recovered both binding capacity (Fig. 4A) and virus production (Table 2). In contrast, no significant changes in the uncoating times were observed during the adaptation to this low degree of cellular shutoff, with very similar times for a 50% uncoating (UT_{50}) among L0, F0.05NA, and F0.05A populations, all of them around 17 to 18 h (Fig. 4E). With regard to the very long adapted population F0.05LA, no significant differences in its binding capacity or in its UT_{50} were observed in comparison with both the F0.05A and L0 populations (Fig. 4A and E), in spite of a significant change in folding (see above; also Fig. 2). Interestingly, during the reversion from 0.05 to 0.00 μg/ml of AMD, the R0NA population did show a statistically significant ($P < 0.05$) decrease in the cell binding capacity (Fig. 4B), which again correlated with a significant decrease ($P < 0.05$) in the virus production per cell (Table 2), and the adapted population R0A recovered both fitness (Table 2) and cell binding capacity (Fig. 4B). Since no changes in the uncoating times were observed in any of the populations adapting to 0.05 μg/ml of AMD and returning to 0.00 μg/ml of AMD (Fig. 4E and F), the observed fitness losses and recoveries could be associated with capsid folding changes affecting the cell binding capacity.

The same analysis was performed during the process of adaptation to 0.2 μg/ml of AMD. Population F0.2NA, which was still nonadapted to the new conditions of high-level cellular shutoff, showed a significant ($P < 0.05$) fitness loss compared to its predecessor population F0.05A (Table 2). Remarkably, this loss did not correlate either with a decrease in the cell binding capacity (Fig. 4C) or with an increase in the uncoating time (Fig. 4G). Instead, it could be due to the cell mortality (90% at 4 days) caused by the high AMD concentration (2). However, the fitness recovery observed in the adapted F0.2A population did correlate with an impressive decrease ($P < 0.005$) in the uncoating time (Fig. 4G), with a UT_{50} of only 3 h compared to 17 h for F0.05A, in spite of a concomitant decrease in the cell binding capacity (Fig. 4C). Additionally, the long-adapted population F0.2LA showed a phenotype with a recovered cell binding capacity and still maintained a short uncoating time (Fig. 4C and G), although fitness remained unaltered. Regarding the reverse process, from 0.2 μg/ml to 0.05 μg/ml of AMD, again fitness loss followed by fitness recovery was observed (Table 2). In this particular case, again, fitness loss could not be explained by a decrease in the cell binding efficiency or a significant increase in the uncoating time (Fig. 4D and H) and not even by toxic side effects affecting cell viability since under this condition of 0.05 μg/ml of AMD cell mortality was much lower. But even more unexpectedly, fitness recovery was not due to an increase in the cell binding capacity or a decrease of the uncoating time (Fig. 4D and H).

Selection of large-plaque-producing populations during the process of adaptation to cellular shutoff. Remarkably, adaptation to cellular shutoff resulted in the selection of large-plaque-producing virus populations (F0.05A, F0.05LA, F0.2A, and F0.2LA populations; Table 2 and Fig. 5) with significantly ($P < 0.001$) larger plaque diameters, which were 3- to 3.5-fold larger than those of the parental virus. These increases in plaque diameter correlated with a significant ($P < 0.01$) increase of the specific infectivity in populations F0.05A and F0.2A (Table 2). However, long-term-adapted F0.05LA and F0.2LA populations decreased again their specific infectivity to basal levels, keeping the plaque diameter unaltered with respect to that of F0.05A and F0.2A populations, respectively (Table 2). Other exceptions were those populations in the process of readaptation to their original conditions (R0NA and R0.05NA) and those already readapted (R0A and R0.05A), which, in spite of showing significantly ($P < 0.01$) increased specific infectivity, kept or even decreased the plaque diameter (Table 2).

As stated above, any change in cellular shutoff conditions was associated with significant ($P < 0.05$) losses in fitness which were recovered after adaptation (Table 2). Interestingly, in most cases these fitness variations positively correlated with plaque diameter

(Table 2). However, while fitness gains were never observed, plaque diameter progressively increased during the processes of adaptation to increasing cellular shutoff. In contrast, during the processes of reversion the plaque diameter never increased (Table 2). In turn, during the process of adaptation to increasing levels of cellular shutoff, fitness recoveries were associated with increases of specific infectivity (Table 2).

Large-plaque-producing populations may emerge because, under conditions of cellular shutoff, more resources are available for the virus. In fact, plaque diameter significantly increased by simply transferring the L0 population to conditions of cellular shutoff (F0.05NA versus L0; Table 2). However, the underlying mechanism of the large-plaque-phenotype selection is much harder to anticipate, as evidenced by the impressive increases after adaptation to shutoff (F0.05A versus F0.05NA and F0.2A versus F0.2NA; Table 2). Understanding the complex dynamics of fitness, specific infectivity, and plaque diameter requires an additional in-depth analysis of the codon usage evolution.

Codon deoptimization versus codon optimization as underlying mechanism of genomic evolution to ensure highest specific infectivity during adaptation to cellular shutoff. In order to explain the unexpected lack of correlation between fitness, specific infectivity, and plaque diameter of the populations selected during the reversion processes as well as of the long-adapted populations, codon usage variations in their mutant spectra were analyzed.

Population F0.05A, selected after 65 passages in the presence of 0.05 μg/ml of AMD, and population F0.2A, selected after 65 passages in the presence of 0.05 μg/ml of AMD and 40 passages in the presence of 0.2 μg/ml of AMD (Fig. 1), evolved through a codon usage deoptimization (Fig. 6A and D) which was characterized by a decrease of codons pairing with anticodons abundantly used by the cell (60% to 100% of use) and an increase of codons pairing with anticodons not abundantly used by the cell (0% to 60% of use). This deoptimization pattern was kept in populations F0.05LA, selected after 120 passages in the presence of 0.05 μg/ml, and F0.2LA, selected after 65 and 70 passages in the presence of 0.05 μg/ml and 0.2 μg/ml of AMD, respectively (Fig. 6B and E). Later on, the latter populations, F0.05LA and F0.2LA, showed an additional codon optimization process (Fig. 6H and K). This codon optimization involved a decrease in codons pairing with anticodons not abundantly used by the cell and an increase in codons pairing with anticodons abundantly used by the cell. This implies a combined process of codon deoptimization/optimization, compared to that of the cell, in the populations long-adapted to both 0.05 and 0.2 μg/ml of AMD. Interestingly, the processes of codon deoptimization (F0.05A and F0.02A) and combined codon deoptimization/optimization (F0.05LA and F0.2LA) correlated, respectively, with significant increases and decreases ($P < 0.05$) of the specific infectivity (Table 2). Populations R0A and R0.05A, which were readapted to their original conditions after 20 passages, showed a very high specific infectivity (Table 2). In the R0A population, a reduction in codon deoptimization (Fig. 6C) and an increase in codon optimization (Fig. 6I) were observed compared with its parental type (F0.05A). However, the adaptation in the reverse processes was toward lower levels of cellular shutoff, the opposite of the situation of the forward processes; hence, interpretations of the biological consequences of codon deoptimization and optimization must therefore be opposed. In summary, the R0A population evolved by mostly deoptimizing its codon usage

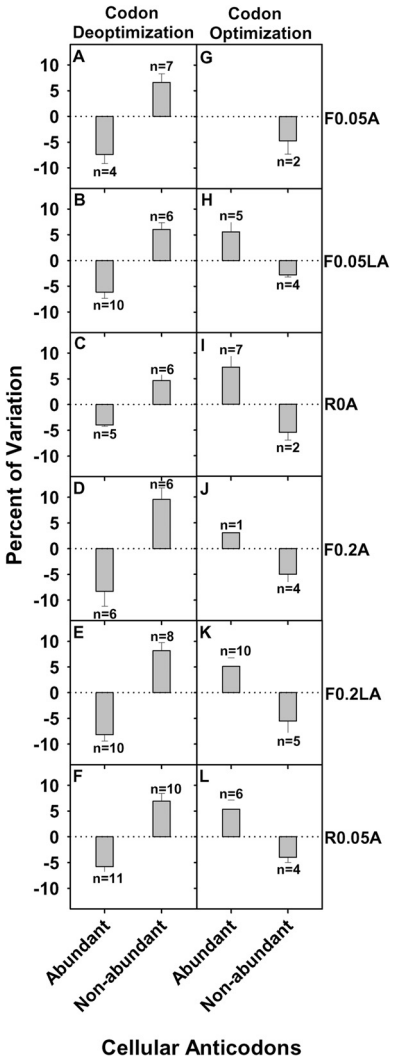

FIG 6 Anticodon usage variation in the capsid region of populations adapted to different conditions of cellular shutoff compared with the parental type L0 population. Codons pairing with anticodons abundantly used by the cell are rarely used by parental type HAV (rare codons), while codons pairing with anticodons not abundantly used by the cell are commonly used by the HAV parental type. Codon usage deoptimization (left column) is defined by a decreased use of codons pairing with anticodons abundantly used by the cell, which are replaced by codons pairing with anticodons not abundantly used by the cell. In contrast, codon usage optimization (right column) is defined by an increased use of codons pairing with anticodons abundantly used by the cell, which correlates with a decrease of use of codons pairing with anticodons not abundantly used by the cell. A total of 63 anticodons exist; thus, a total of 50 anticodons in F0.05A, 38 in F0.05LA, 43 in R0A, 46 in F0.2A, 30 in F0.2LA, and 32 in R0.05A populations do not vary their use in respect to the L0 population. Populations are described in Fig. 1.

to adapt to conditions of noncellular shutoff and this correlated with a high specific infectivity. To what extent the evolving process of R0.05A population was also driven by a codon deoptimization is much harder to evaluate due to the complex codon usage variation of its parental population (F0.2LA). Furthermore, a reduction in the specific infectivity after additional passages under conditions of no shutoff cannot be ruled out.

In addition, the CpG and UpA content of the genomic capsid region tended to decrease during the process of adaptation to

TABLE 3 Potential generation of mutations inducing codon usage changes in the HAV capsid coding region

Type of mutation[a]	No. by frequency class[b]:			
	Same	Lower	Higher	Total
Syn T_s	76	281	450	807
Nsyn T_s	677	519	312	1,508
Syn T_v	116	384	287	787
Nsyn T_v	1,626	1,065	970	3,661
Total	2,495	2,249	2,019	6,763

[a] Mutations are classified as synonymous (Syn) or nonsynonymous (NSyn) and as transitions (T_s) or transversions (T_v).
[b] The new generated codons after mutation are classified as belonging to the same-frequency class (within a 10% range), a lower-frequency class (below 10%), or a higher-frequency class (above 10%) compared with the original ones with respect to cell host codon usage.

cellular shutoff. At the quasispecies level, the average CpG and UpA numbers per sequence, in the VP1 and VP3 fragments analyzed, suffered very small variations, from 3 to 2 and from 35 to 34, respectively.

The need to change the codon usage combined with the transition mutation bias and the HAV capsid genomic composition explains the amino acid replacements selected during the adaptation to the different conditions of cellular shutoff. Many of the mutations that appeared during the processes of adaptation to changing conditions of cellular shutoff induced codon usage changes but also amino acid replacements, which in turn may explain the changes in capsid folding and function. Nevertheless, while the same amino acid sequences were shared in each pair of the populations L0/F0.05NA, F0.05A/F0.2NA, F0.05A/R0NA, and F0.2LA/R0.05NA, differences in MAb recognition patterns (Fig. 2), physical stabilities (Fig. 3), and cell binding capacities/uncoating times (Fig. 4) were shown, indicating that shutoff conditions play an important role in capsid folding and function, eventually driven by codon usage.

In an attempt to explain these amino acid replacements, an analysis of all potential mutations in the capsid region of the pHM175 43c strain of HAV was undertaken. Mutations were classified as synonymous (Syn) or nonsynonymous (NSyn) and as transitions (T_s) or transversions (T_v). Additionally, the newly generated codons were sorted as being similarly frequent (within a 10% range), less frequent (below 10%), or more frequent (above 10%) than the original ones with respect to the cell host codon usage. The process of adaptation to cellular shutoff involved, as stated above, a dominant process of codon deoptimization combined thereafter with a process of codon optimization (Fig. 6). Due to the specific genomic composition of the HAV capsid region, the likelihood of generation of a new codon belonging to a less frequent class than the original one (deoptimization) by random mutation, taking into account that the T_s/T_v ratio in HAV is around 3 (34), is higher with Nsyn T_s than with any other kind of mutation, followed by Nsyn T_v (Table 3). In fact, during the codon deoptimization process over 75% of the mutations in the quasispecies induced a change to a lower-frequency-class codon and most of them were indeed Nsyn. In contrast, the random generation of a codon belonging to a higher-frequency class than the original one (optimization) is higher with Syn T_s, and the quasispecies analyses revealed that most of the mutations associated with the optimization process were Syn.

DISCUSSION

The degeneracy of the genetic code makes possible an amazingly large number of different nucleotide sequences encoding a given protein. In the particular case of the HAV capsid polyprotein, its 791-amino-acid-long sequence can be encoded by 3.8×10^{395} different RNA sequences, all of them translating exactly the same protein sequence (determined as described in reference 35). Additionally, the number of RNA sequences among the swarm of mutants of HAV could even be higher, since there are amino acid positions that allow several alternatives (34). The typical quasispecies dynamics, with the continuous generation of competing viral genomes and the selection of the fittest mutant distribution in a given environment, contributes to dynamically shape the actual sequence space (36). Among the selective constraints that limit the diversity of the mutant distributions of the HAV capsid coding region, the bottlenecks imposed during the biological cycle in the host are noteworthy (22, 27), as well as the need to finely control the translation kinetics in this specific genomic region through the use of clusters of rare codons which define translation attenuation patterns (15, 17). The particular codon usage (codon bias) of an organism reflects the evolutionary forces acting within its genome (37, 38) and contributes to drastically reducing the actual sequence space. In the virus world, at least four mechanisms underlying such a bias exist: mutational bias or the specific nucleotide composition (39–42); translation selection, or the optimal codon adaptation to the tRNA pool in order to get a highly efficient and accurate translation (43–47); fine-tuning translation kinetics selection, or the right combination of abundant and rare codons to allow a regulated ribosome traffic rate that temporally separates protein folding events, ensuring "beneficial" and avoiding "unwanted" interactions within the growing peptide (17); and selection for mechanisms to escape the antiviral cell responses (48, 49). Except the last, all these mechanisms are shared in all organisms (50), and it is likely that a combination of all of them is the actual evolutionary force shaping the codon usage of HAV. In fact, HAV shows an extremely low CpG content (35, 51, 52) that can be related to the need to avoid as much as possible the antiviral cell responses (53) and which, together with the genomic composition (51, 53) and the regulation of the translation kinetics (17), contributes to the final codon usage outcome. Fine-tuning translation kinetics selection has been predicted through genomic proxies (17), and in the present study, the relationship between codon usage and protein folding in the capsid region was investigated.

Remarkably, any change in cellular protein synthesis shutoff conditions induced significant modifications of capsid folding, as can be seen through the antigenic structure. These modifications were also observed in the physical properties of the capsids, and during the adaptation to increasing levels of cellular shutoff, there was a general tendency toward the loss of the otherwise highly stable phenotype of HAV at high temperature, at low pH, and in the presence of biliary salts. The phenotype of the population long adapted to a high level of cellular shutoff was more similar to that of other picornaviruses than to that of the parental HAV (54–56). However, as predicted by the quasispecies theory (57), each population evolved in a particular manner in each specific environment as evidenced during the processes of readaptation to the original conditions. Accordingly, while the distribution of codons into the different-frequency classes was reverted, some particular genomes with mutations involved in the process of adaptation to

cellular shutoff were rapidly replaced as a result of the quasispecies memory (58, 59), but other genomes with compensatory mutations emerged, and consequently, the readapted populations did not always recover the original capsid phenotypes. In contrast, fitness, understood as the production of infectious viruses, was always recovered although it never increased. Fitness is the ultimate goal of selection, and in the particular case of HAV adaptation to different conditions of cellular shutoff, this selection is exerted through adaptation of its capsid codon usage, which in turn affects capsid folding and function.

The influence of the level of codon optimization in the variations of HAV specific infectivity is remarkable, and while in poliovirus codon-deoptimized viruses show lower specific infectivity (60, 61), in HAV the contrary is the rule. HAV has evolved to a naturally deoptimized codon usage (16) and a very high specific infectivity (around 1/25) compared with other picornaviruses (60–62). HAV genomic adaptation to cellular shutoff followed a two-phase pattern consisting, first, of codon deoptimization, whose underlying pressure must be the control of the translation kinetics, followed thereafter by codon optimization, whose underlying pressure must be a highly efficient translation. Experiments are in progress to test the influence of the different codon usage patterns of the different populations on the speed of translation. Codon deoptimization (populations F0.05A, F0.2A, and R0A) correlated with increases (up to 1/2) in the specific infectivity, while an initial deoptimization followed by codon optimization (populations F0.05LA and F0.2LA) correlated with decreases (down to parental levels) in specific infectivity. However, population R0.05A did show a very high specific infectivity, in spite of a mixed pattern of codon variation. Nonetheless, the biological consequence of this complex pattern, which reflects the memory of the quasispecies (56), is very difficult to evaluate. Additionally, as stated above, adaptation to changing levels of cellular shutoff is a two-phase process. During the first phase, there is the need to be highly efficient (high specific infectivity) to overcome a very critical change. This first phase was shown in populations F0.05A and F0.2A and in populations R0A and R0.05A. During the second phase, once the first adaptation process was completed, F0.05LA and F0.2LA populations continued to evolve without the need to be highly efficient (low specific infectivity). This second phase could not be evaluated during the reverse processes, since long-adapted populations were not obtained.

Capsid folding greatly contributes not only to fitness but also to specific infectivity. What determines the latter parameter, which is defined as the ratio between infectious and physical particles and provides an indication of the number of particles required to achieve an infectious cycle, is far from clear. Failures at any step during an infectious cycle may lead to an abortive cycle (61). These failures may be at the level of receptor binding, internalization and uncoating, initiation of genome translation, translation elongation, RNA replication, capsid formation, RNA encapsidation, and capsid maturation. Specific infectivity is environment dependent (57), and consequently, the observed variations during adaptation to different conditions of cellular shutoff are not surprising.

HAV has a very inefficient internal ribosome entry site (IRES) (14) whose activity should be coupled with a proper translation rate to avoid decompensation events. A single mutation at position 513 (A to G) of the IRES region appeared in population F0.2A and was conserved thereafter (sequences available at GenBank). However, this replacement should not induce any significant change in the IRES structure due to the G:U wobble base pair, indicating that the initiation of translation did not play a critical role in the adaptation to the different shutoff conditions. Only one mutation was detected in the coding regions for the 3C protease and the 3D polymerase. Mutation A39V in the 3D polymerase appeared in population F0.05A and was maintained thereafter (sequences available at GenBank). This mutation is located close to the previously described F42L, which was associated with an increase in RNA replication (63). However, mutation A39V was not essential for the process of adaptation to the different cellular shutoff conditions since it did not correlate either with an increase of RNA replication or with the specific infectivity changes observed during the adaptation to high levels of cellular shutoff or during the reverse process to low levels of cellular shutoff or with fitness. Additionally, the substitution maintained a motif found across the *Picornaviridae* family since it changed from PAA (HAV and foot-and-mouth-disease virus) to PAV (enterovirus and rhinovirus).

It has been previously described that uncoating in HAV is asynchronic and extremely inefficient (64), in correlation with the here-observed UT_{50} of the parental type of around 18 h. The populations adapted to high levels of cellular shutoff showed a much more efficient uncoating process, with a UT_{50} of around 3 to 8 h, much closer to the 30 min described for poliovirus (65). Amazingly, during the process of adaptation to cellular shutoff, large-plaque-producing populations were selected, the largest being those with the shorter uncoating times, with diameters similar to those of poliovirus (66). However, next to them were populations adapted to low levels of cellular shutoff with uncoating times identical to those of the parental type, indicating that the diameter correlated with the level of codon deoptimization rather than with the uncoating time and that uncoating time was actually the consequence of the level of codon deoptimization.

The high proportion of amino acid replacements which occurred associated with the process of codon usage deoptimization may be explained by the genomic composition of the HAV P1 region combined with the high T_s/T_v rate. These replacements affected residues encoded by rare codons highly exposed at the capsid surface (17), where the tolerance to amino acid substitutions must be higher. On the other hand, rare codons are by definition low fidelity due to erroneous incorporations of near-cognate tRNAs during the long search for the low-concentration cognate tRNAs (1, 4, 5). The residues encoded by these low-fidelity rare codons are supposed to be located at sites free of structural constraints such as the outer capsid surface, and indeed, 67% of residues encoded by rare codons in the HAV capsid region are exposed at the capsid surface on the existing models (15). Interestingly, these rare codons at the capsid surface are located around the epitopes, and their replacement under normal conditions of no cellular shutoff is prevented even under the immune pressure of the MAbs K34C8 and H7C27 (67), which, however, does not eliminate the possibility of amino acid replacements due to their low-fidelity character. In contrast, these same rare codons are frequently replaced by nonsynonymous codons under conditions of cellular shutoff even without immune pressure. Hence, these nonsynonymous replacements must play a role in the antigenic changes associated with the changing cellular-shutoff conditions. However, codon usage by itself must also influence capsid folding as evidenced by the alteration of the antigenic and physical struc-

ture and function of capsids of still-nonadapted populations which did not show any changes at the genomic level. In contrast, the optimization process was characterized by a high proportion of synonymous mutations at sites encoded by rare codons but buried inside the capsid (15).

AMD may have numerous effects on the cell, including alterations in the levels of proteins involved in innate immunity. This alteration in virus-sensing proteins could affect the ability of the virus to infect and spread, possibly affecting plaque size. It has been suggested that the phenotypic effects of altering codon usage frequencies may be caused by the altered frequencies of dinucleotide pairs (60), particularly CpG and sometimes UpA, which are underrepresented in viral genomes (52). The decrease of CpG motifs in an A/U-rich background has been proposed to be a viral strategy to avoid the innate immune system (68). On the other hand, UpA dinucleotides are direct substrates for cleavage of single-stranded RNA by the antiviral RNase L (69). Both mechanisms altogether would lead to greater fitness and more virus spread. In fact, poliovirus infectivity has been greatly reduced by increasing the frequencies of CpG and UpA dinucleotides (66). Under shutoff conditions, an altered (decreased) innate response would be expected and thus an increase of the CpG and UpA content. However, in the particular case of HAV, the adaptation to cellular shutoff was associated with a very small decrease in the number of CpG and UpA dinucleotides, suggesting that the codon usage changes observed were not the consequence of a selection control over the frequencies of these dinucleotides.

Overall, the process of adaptation/reversion of HAV to conditions of increasing/decreasing cellular shutoff was driven by dynamic changes in codon usage of the capsid coding region, which would relocate the mutant spectra to positions in the sequence space with different fitness (70), through changes in the capsid conformation critical for its folding, stability, and function. HAV codon usage constitutes an additional example of what seems to be a broader phenomenon, as revealed by the role of nonoptimal codons in the control of the circadian cycle of both prokaryotes (71) and eukaryotes (72) or even the cell cycle in eukaryotes (73).

ACKNOWLEDGMENTS

This work was supported in part by Spanish Ministry of Science and Innovation and Ministry of Economy projects BIO2008-01312 and BIO2011-23461, respectively, and by Generalitat de Catalunya project 2009SGR00024 and the Biotechnology Reference Network (XRB). M. Isabel Costafreda, Francisco J. Pérez-Rodríguez, and Lucía D'Andrea were recipients of fellowships from the Spanish Ministries of Science, Education, and External Affairs and Cooperation, respectively.

REFERENCES

1. **Gingold H, Pilpel Y.** 2011. Determinants of translation efficiency and accuracy. Mol. Syst. Biol. **7:**481. http://dx.doi.org/10.1038/msb.2011.14.
2. **Kramer G, Boehringer D, Ban N, Bukau B.** 2009. The ribosome as a platform for co-translational processing, folding and targeting of newly synthesized proteins. Nat. Struct. Mol. Biol. **16:**589–597. http://dx.doi.org/10.1038/nsmb.1614.
3. **Komar AA.** 2009. A pause for thought along the co-translational folding pathway. Trends Biochem. Sci. **34:**16–24. http://dx.doi.org/10.1016/j.tibs.2008.10.002.
4. **Plant EP, Nguyen P, Russ JR, Pittman YR, Nguyen T, Quesinberry JT, Kinzy TG, Dinman JD.** 2007. Differentiating between near- and non-cognate codons in *Saccharomyces cerevisiae*. PLoS One **2:**e517. http://dx.doi.org/10.1371/journal.pone.0000517.
5. **Kramer EB, Farabaugh PJ.** 2007. The frequency of translational misreading errors in E. coli is largely determined by tRNA competition. RNA **13:**87–96. http://dx.doi.org/10.1261/rna.294907.
6. **Zhou T, Weems M, Wilke CO.** 2009. Translationally optimal codons associate with structurally sensitive sites in proteins. Mol. Biol. Evol. **26:**1571–1580. http://dx.doi.org/10.1093/molbev/msp070.
7. **Zhang G, Ignatova Z.** 2009. Generic algorithm to predict the speed of translational elongation: implications for protein biogenesis. PLoS One **4:**e5036. http://dx.doi.org/10.1371/journal.pone.0005036.
8. **Widmann M, Clairo M, Dippon J, Pleiss J.** 2008. Analysis of the distribution of functionally relevant rare codons. BMC Genomics **9:**207. http://dx.doi.org/10.1186/1471-2164-9-207.
9. **Cooper GM, Brown CD.** 2008. Qualifying the relationship between sequence conservation and molecular function. Genome Res. **18:**201–205. http://dx.doi.org/10.1101/gr.7205808.
10. **Zhang G, Ignatova Z.** 2011. Folding at the birth of the nascent chain: coordinating translation with co-translational folding. Curr. Opin. Struct. Biol. **21:**25–31. http://dx.doi.org/10.1016/j.sbi.2010.10.008.
11. **Zhang G, Hubalewska M, Ignatova Z.** 2009. Transient ribosomal attenuation coordinates protein synthesis and co-translational folding. Nat. Struct. Mol. Biol. **16:**274–280. http://dx.doi.org/10.1038/nsmb.1554.
12. **Kimchi-Sarfaty C, Oh JM, Kim IW, Sauna ZE, Calcagno AM, Ambudkar SV, Gottesman MM.** 2007. A "silent" polymorphism in the MDR1 gene changes substrate specificity. Science **315:**525–528. http://dx.doi.org/10.1126/science.1135308.
13. **Ali IK, McKendrick L, Morley SJ, Jackson RJ.** 2001. Activity of the hepatitis A virus IRES requires association between the cap-binding translation initiation factor (eIF4E) and eIF4G. J. Virol. **75:**7854–7863. http://dx.doi.org/10.1128/JVI.75.17.7854-7863.2001.
14. **Whetter LE, Day SP, Elroystein O, Brown EA, Lemon SM.** 1994. Low efficiency of the 5′ nontranslated region of hepatitis A virus RNA in directing cap-independent translation in permissive monkey kidney cells. J. Virol. **68:**5253–5263.
15. **Sanchez G, Bosch A, Pintó RM.** 2003. Genome variability and capsid structural constraints of hepatitis A virus. J. Virol. **77:**452–459. http://dx.doi.org/10.1128/JVI.77.1.452-459.2003.
16. **Pintó RM, Aragones L, Costafreda MI, Ribes E, Bosch A.** 2007. Codon usage and replicative strategies of hepatitis A virus. Virus Res. **127:**158–163. http://dx.doi.org/10.1016/j.virusres.2007.04.010.
17. **Aragonès L, Guix S, Ribes E, Bosch A, Pintó RM.** 2010. Fine-tuning translation kinetics selection as the driving force of codon usage bias in the hepatitis A virus capsid. PLoS Pathog. **6:**e1000797. http://dx.doi.org/10.1371/journal.ppat.1000797.
18. **Geller R, Vignuzzi M, Andino R, Frydman J.** 2007. Evolutionary constraints on chaperone-mediated folding provide an antiviral approach refractory to development of drug resistance. Genes Dev. **21:**195–205. http://dx.doi.org/10.1101/gad.1505307.
19. **Geller R, Taguwa S, Frydman J.** 2012. Broad action of Hsp90 as a host chaperone required for viral replication. Biochim. Biophys. Acta **1823:**698–706. http://dx.doi.org/10.1016/j.bbamcr.2011.11.007.
20. **Reich E, Franklin RM, Shatkin AJ, Tatumel.** 1962. Action of actinomycin D on animal cells and viruses. Proc. Natl. Acad. Sci. U. S. A. **48:**1238–1245. http://dx.doi.org/10.1073/pnas.48.7.1238.
21. **Costafreda MI, Bosch A, Pintó RM.** 2006. Development, evaluation, and standardization of a real-time TaqMan reverse transcription-PCR assay for quantification of hepatitis A virus in clinical and shellfish samples. Appl. Environ. Microbiol. **72:**3846–3855. http://dx.doi.org/10.1128/AEM.02660-05.
22. **Costafreda MI, Ribes E, Franch A, Bosch A, Pintó RM.** 2012. A single mutation in the glycophorin A binding site of hepatitis A virus enhances virus clearance from the blood and results in a lower fitness variant. J. Virol. **86:**7887–7895. http://dx.doi.org/10.1128/JVI.00707-12.
23. **Pintó RM, Costafreda MI, Bosch A.** 2009. Risk assessment in shellfish-borne outbreaks of hepatitis A. Appl. Environ. Microbiol. **75:**7350–7355. http://dx.doi.org/10.1128/AEM.01177-09.
24. **Cromeans T, Sobsey MD, Fields HA.** 1987. Development of a plaque assay for a cytopathic, rapidly replicating isolate of hepatitis A virus. J. Med. Virol. **22:**45–56. http://dx.doi.org/10.1002/jmv.1890220107.
25. **Bishop NE, Hugo DL, Borovec SV, Anderson DA.** 1994. Rapid and efficient purification of hepatitis-A virus from cell-culture. J. Virol. Methods **47:**203–216. http://dx.doi.org/10.1016/0166-0934(94)90078-7.
26. **Ping LH, Lemon SM.** 1992. Antigenic structure of human hepatitis A virus defined by analysis of escape mutants selected against murine monoclonal antibodies. J. Virol. **66:**2208–2216.

27. **Sanchez G, Aragonès L, Costafreda MI, Ribes E, Bosch A, Pintó RM.** 2004. Capsid region involved in hepatitis a virus binding to glycophorin A of the erythrocyte membrane. J. Virol. **78:**9807–9813. http://dx.doi.org/10.1128/JVI.78.18.9807-9813.2004.
28. **Stapleton JT, Raina V, Winokur PL, Walters K, Klinzman D, Rosen E, McLinden JH.** 1993. Antigenic and immunogenic properties of recombinant hepatitis A virus 14S and 70S subviral particles. J. Virol. **67:**1080–1085.
29. **Bosch A, Gonzalez-Dankaart JF, Haro I, Gajardo R, Perez JA, Pintó RM.** 1998. A new continuous epitope of hepatitis A virus. J. Med. Virol. **54:**95–102. http://dx.doi.org/10.1002/(SICI)1096-9071(199802)54:2<95::AID-JMV5>3.0.CO;2-J.
30. **Lemon SM, Murphy PC, Shields PA, Ping LH, Feinstone SM, Cromeans T, Jansen RW.** 1991. Antigenic and genetic variation in cytopathic hepatitis A virus variants arising during persistent infection: evidence for genetic recombination. J. Virol. **65:**2056–2065.
31. **Pintó RM, Guix S, Gonzalez-Dankaart JF, Caballero S, Sanchez G, Guo KJ, Ribes E, Bosch A.** 2002. Hepatitis A virus polyprotein processing by Escherichia coli proteases. J. Gen. Virol. **83:**359–368.
32. **Crowther D, Melnick JL.** 1961. The incorporation of neutral red and acridine orange into developing poliovirus particles making them photosensitive. Virology **14:**11–21. http://dx.doi.org/10.1016/0042-6822(61)90127-1.
33. **dos Reis M, Savva R, Wernisch L.** 2004. Solving the riddle of codon usage preferences: a test for translational selection. Nucleic Acids Res. **32:**5036–5044. http://dx.doi.org/10.1093/nar/gkh834.
34. **Sanchez G, Bosch A, Gomez-Mariano G, Domingo E, Pintó RM.** 2003. Evidence for quasispecies distributions in the human hepatitis A virus genome. Virology **315:**34–42. http://dx.doi.org/10.1016/S0042-6822(03)00483-5.
35. **Bosch A, Mueller S, Pintó RM.** 2010. Codon biases and viral fitness, p 271–283. *In* Ehrenfeld E, Domingo E, Roos R (ed), The picornaviruses. ASM Press, Washington, DC.
36. **Perales C, Martin V, Ruiz-Jarabo CM, Domingo E.** 2005. Monitoring sequence space as a test for the target of selection in viruses. J. Mol. Biol. **345:**451–459. http://dx.doi.org/10.1016/j.jmb.2004.10.066.
37. **Grantham R, Gautier C, Gouy M.** 1980. Codon frequencies in 119 individual genes confirm consistent choices of degenerate bases according to genome type. Nucleic Acids Res. **8:**1893–1912. http://dx.doi.org/10.1093/nar/8.9.1893.
38. **Grantham R, Gautier C, Gouy M, Mercier R, Pave A.** 1980. Codon catalog usage and the genome hypothesis. Nucleic Acids Res. **8:**r49–r62.
39. **Ma MR, Ha XQ, Ling H, Wang ML, Zhang FX, Zhang SD, Li G, Yan W.** 2011. The characteristics of the synonymous codon usage in hepatitis B virus and the effects of host on the virus in codon usage pattern. Virol. J. **8:**544. http://dx.doi.org/10.1186/1743-422X-8-544.
40. **Jenkins GM, Pagel M, Gould EA, de A Zanotto PM, Holmes EC.** 2001. Evolution of base composition and codon usage bias in the genus Flavivirus. J. Mol. Evol. **52:**383–390. http://dx.doi.org/10.1007/s002390010168.
41. **Jenkins GM, Holmes EC.** 2003. The extent of codon usage bias in human RNA viruses and its evolutionary origin. Virus Res. **92:**1–7. http://dx.doi.org/10.1016/S0168-1702(02)00309-X.
42. **Hu JS, Wang QQ, Zhang J, Chen HT, Xu ZW, Zhu L, Ding YZ, Ma LN, Xu K, Gu YX, Liu YS.** 2011. The characteristic of codon usage pattern and its evolution of hepatitis C virus. Infect. Genet. Evol. **11:**2098–2102. http://dx.doi.org/10.1016/j.meegid.2011.08.025.
43. **Zhao KN, Chen J.** 2011. Codon usage roles in human papillomavirus. Rev. Med. Virol. **21:**397–411. http://dx.doi.org/10.1002/rmv.707.
44. **Zhi N, Wan Z, Liu X, Wong S, Kim DJ, Young NS, Kajigaya S.** 2010. Codon optimization of human parvovirus B19 capsid genes greatly increases their expression in nonpermissive cells. J. Virol. **84:**13059–13062. http://dx.doi.org/10.1128/JVI.00912-10.
45. **Karlin S, Blaisdell BE, Schachtel GA.** 1990. Contrasts in codon usage of latent versus productive genes of Epstein-Barr virus: data and hypotheses. J. Virol. **64:**4264–4273.
46. **Zhou J, Liu WJ, Peng SW, Sun XY, Frazer I.** 1999. Papillomavirus capsid protein expression level depends on the match between codon usage and tRNA availability. J. Virol. **73:**4972–4982.
47. **Cladel NM, Budgeon LR, Hu J, Balogh KK, Christensen ND.** 2013. Synonymous codon changes in the oncogenes of the cottontail rabbit papillomavirus lead to increased oncogenicity and immunogenicity of the virus. Virology **438:**70–83. http://dx.doi.org/10.1016/j.virol.2013.01.005.
48. **Sugiyama T, Gursel M, Takeshita F, Coban C, Conover J, Kaisho T, Akira S, Klinman DM, Ishii KJ.** 2005. CpG RNA: identification of novel single-stranded RNA that stimulates human CD14+CD11c+ monocytes. J. Immunol. **174:**2273–2279.
49. **Takeshita F, Gursel I, Ishii KJ, Suzuki K, Gursel M, Klinman DM.** 2004. Signal transduction pathways mediated by the interaction of CpG DNA with Toll-like receptor 9. Semin. Immunol. **16:**17–22. http://dx.doi.org/10.1016/j.smim.2003.10.009.
50. **Hershberg R, Petrov DA.** 2008. Selection on codon bias. Annu. Rev. Genet. **42:**287–299. http://dx.doi.org/10.1146/annurev.genet.42.110807.091442.
51. **D' Andrea L, Pintó RM, Bosch A, Musto H, Cristina J.** 2011. A detailed comparative analysis on the overall codon usage patterns in hepatitis A virus. Virus Res. **157:**19–24. http://dx.doi.org/10.1016/j.virusres.2011.01.012.
52. **Greenbaum BD, Levine AJ, Bhanot G, Rabadan R.** 2008. Patterns of evolution and host gene mimicry in influenza and other RNA viruses. PLoS Pathog. **4:**e1000079. http://dx.doi.org/10.1371/journal.ppat.1000079.
53. **Pintó RM, D'Andrea L, Perez-Rodriguez FJ, Costafreda MI, Ribes E, Guix S, Bosch A.** 2012. Hepatitis A virus evolution and the potential emergence of new variants escaping the presently available vaccines. Future Microbiol. **7:**331–346. http://dx.doi.org/10.2217/fmb.12.5.
54. **Scholz E, Heinricy U, Flehmig B.** 1989. Acid stability of hepatitis A virus. J. Gen. Virol. **70:**2481–2485. http://dx.doi.org/10.1099/0022-1317-70-9-2481.
55. **Siegl G, Weitz M, Kronauer G.** 1984. Stability of hepatitis A virus. Intervirology **22:**218–226. http://dx.doi.org/10.1159/000149554.
56. **Siegl G, Frosner GG, Gauss-Muller V, Tratschin JD, Deinhardt F.** 1981. The physicochemical properties of infectious hepatitis A virions. J. Gen. Virol. **57:**331–341. http://dx.doi.org/10.1099/0022-1317-57-2-331.
57. **Domingo E, Sheldon J, Perales C.** 2012. Viral quasispecies evolution. Microbiol. Mol. Biol. Rev. **76:**159–216. http://dx.doi.org/10.1128/MMBR.05023-11.
58. **Ruiz-Jarabo CM, Arias A, Baranowski E, Escarmis C, Domingo E.** 2000. Memory in viral quasispecies. J. Virol. **74:**3543–3547. http://dx.doi.org/10.1128/JVI.74.8.3543-3547.2000.
59. **Ruiz-Jarabo CM, Arias A, Molina-Paris C, Briones C, Baranowski E, Escarmis C, Domingo E.** 2002. Duration and fitness dependence of quasispecies memory. J. Mol. Biol. **315:**285–296. http://dx.doi.org/10.1006/jmbi.2001.5232.
60. **Burns CC, Shaw J, Campagnoli R, Jorba J, Vincent A, Quay J, Kew O.** 2006. Modulation of poliovirus replicative fitness in HeLa cells by deoptimization of synonymous codon usage in the capsid region. J. Virol. **80:**3259–3272. http://dx.doi.org/10.1128/JVI.80.7.3259-3272.2006.
61. **Mueller S, Papamichail D, Coleman JR, Skiena S, Wimmer E.** 2006. Reduction of the rate of poliovirus protein synthesis through large-scale codon deoptimization causes attenuation of viral virulence by lowering specific infectivity. J. Virol. **80:**9687–9696. http://dx.doi.org/10.1128/JVI.00738-06.
62. **Graci JD, Gnädig NF, Galarraga JE, Castro C, Vignuzzi M, Cameron CE.** 2012. Mutational robustness of an RNA virus influences sensitivity to lethal mutagenesis. J. Virol. **86:**2869–2873. http://dx.doi.org/10.1128/JVI.05712-11.
63. **Konduru K, Kaplan GG.** 2010. Determinants in 3Dpol modulate the rate of growth of hepatitis A virus. J. Virol. **84:**8342–8347. http://dx.doi.org/10.1128/JVI.01470-09.
64. **Bishop NE, Anderson DA.** 2000. Uncoating kinetics of hepatitis A virus virions and provirions. J. Virol. **74:**3423–3426. http://dx.doi.org/10.1128/JVI.74.7.3423-3426.2000.
65. **Brandenburg B, Lee LY, Lakadamyali M, Rust MJ, Zhuang X, Hogle JM.** 2007. Imaging poliovirus entry in live cells. PLoS Biol. **5:**e183. http://dx.doi.org/10.1371/journal.pbio.0050183.
66. **Burns CC, Campagnoli R, Shaw J, Vincent A, Jorba J, Kew O.** 2009. Genetic inactivation of poliovirus infectivity by increasing the frequencies of CpG and UpA dinucleotides within and across synonymous capsid region codons. J. Virol. **83:**9957–9969. http://dx.doi.org/10.1128/JVI.00508-09.
67. **Aragonès L, Bosch A, Pintó RM.** 2008. Hepatitis A virus mutant spectra under the selective pressure of monoclonal antibodies: codon usage constraints limit capsid variability. J. Virol. **82:**1688–1700. http://dx.doi.org/10.1128/JVI.01842-07.
68. **Jimenez-Baranda S, Greenbaum B, Manches O, Handler J, Rabadan R,**

Levine A, Bhardwaj N. 2011. Oligonucleotide motifs that disappear during the evolution of influenza virus in humans increase alpha interferon secretion by plasmacytoid dendritic cells. J. Virol. **85:**3893–3904. http://dx.doi.org/10.1128/JVI.01908-10.

69. **Duan J, Antezana M.** 2003. Mammalian mutation pressure, synonymous codon choice, and mRNA degradation. J. Mol. Evol. **57:**694–701. http://dx.doi.org/10.1007/s00239-003-2519-1.
70. **Lauring AS, Acevedo A, Cooper SB, Andino R.** 2012. Codon usage determines the mutational robustness, evolutionary capacity, and virulence of an RNA virus. Cell Host Microbe **12:**623–632. http://dx.doi.org/10.1016/j.chom.2012.10.008.
71. **Xu Y, Ma P, Shah P, Rokas A, Liu Y, Johnson CH.** 2013. Non-optimal codon usage is a mechanism to achieve circadian clock conditionality. Nature **495:**116–120. http://dx.doi.org/10.1038/nature11942.
72. **Zhou M, Guo J, Cha J, Chae M, Chen S, Barral JM, Sachs MS, Liu Y.** 2013. Non-optimal codon usage affects expression, structure and function of clock protein FRQ. Nature **495:**111–115. http://dx.doi.org/10.1038/nature11833.
73. **Frenkel-Morgenstern M, Danon T, Christian T, Igarashi T, Cohen L, Hou YM, Jensen LJ.** 2012. Genes adopt non-optimal codon usage to generate cell cycle-dependent oscillations in protein levels. Mol. Syst. Biol. **8:**572. http://dx.doi.org/10.1038/msb.2012.3.